Josephson and noise scanning tunneling microscopy on conventional, unconventional and disordered superconductors

Chatzopoulos, D.

3

Inhomogeneous superfluid density in Fe(Te,Se)

Although the possibility of spatial variations in the superfluid of unconventional, strongly correlated superconductors has been suggested [1–7] it is not known whether such inhomogeneities—if they exist—are driven by disorder, strong scattering or other factors. In this chapter we employ atomic-resolution Josephson scanning tunnelling microscopy to reveal a strongly inhomogeneous superfluid in the iron-based superconductor $FeTe_{0.55}Se_{0.45}$. By simultaneously measuring the topographic and electronic properties of the superconductor, we find that this inhomogeneity in the superfluid is not caused by structural disorder or strong inter-pocket scattering and is not correlated with variations in the energy required to break electron pairs. Instead, we see a clear spatial correlation between the superfluid density and the quasi-particle strength (the height of the coherence peak) on a local scale. This result places iron-based superconductors on equal footing with copper oxide superconductors, where a similar relation has been observed on the macroscopic scale. Our results establish the existence of strongly inhomogeneous superfluids in unconventional superconductors and shed light on the relation between quasiparticle character and superfluid density. When repeated at different temperatures, our technique could further help to elucidate what local and global mechanisms limit the critical temperature in unconventional superconductors.

3.1. Introduction

Superconductivity emerges when electrons pair up to form Cooper pairs and then establish phase coherence to condense into a macroscopic quantum state, the superfluid. Cooper pairing is governed by the binding energy of the pairs, Δ_{CP}, and the phase coherence (or stiffness) governs the superfluid density [1], n_{SF}. For conventional superconductors, like aluminium or lead, the superfluid density is spatially homogeneous because the lattice constant is much smaller than the size of the Cooper pair (usually hundreds of nanometres) and because the large superfluid density guarantees a high phase stiffness. As we have already hinted in Chapter 1, unconventional, strongly correlated superconductors are very different from conventional superconductors for the following reasons:

- The size of the Cooper pairs, which is roughly given by the coherence length, is generally smaller.

- The superfluid density is smaller.

- Higher disorder exists, owing to dopant atoms or intrinsic tendencies for phase separation or charge order.

- The sign of the superconducting gap changes.

Despite much progress [2, 8], we lack a theoretical understanding of strongly correlated superconductors. It has been proposed that, in principle, spatial variations can exist in the superfluid density [3, 4]. Very similar ideas have been discussed thoroughly in the context of superconductor–insulator transitions [5–7] or Bose–Einstein condensation of electronic liquids [9]. However, little is known about the local physics in such systems because of the technical challenges associated with visualizing the superfluid density on the atomic scale, especially when simultaneously probing the density of states to investigate the origin of the inhomogeneity.

3.2. Theory of tunneling between superconductors

The pair-breaking gap (the energy required to break a Cooper pair) and the superfluid density should be accessible through two distinct spectroscopic signatures in a tunnelling junction between superconductors (Fig. 3.1a). The first one is visible in the single-particle channel, where Bogoliubov quasiparticles with energies larger than the pair-breaking gaps transport the charge, as shown in Fig. 3.1b. In the case of the scanning tunnelling microscopy (STM) configuration relevant to this experiment, one of the superconductors is the tip (with gap $\Delta_{\mathrm{CP,t}}$) and the other is the sample (with gap $\Delta_{\mathrm{CP,s}}$), leading to a total energy gap of $2(\Delta_{\mathrm{CP,t}} + \Delta_{\mathrm{CP,s}})$ (Fig. 3.1c). The second spectroscopic feature is observed at bias energies close to the Fermi energy, E_{F}, where one can access the Cooper pair channel that yields information about the superfluid density. Voltage-biased Josephson tunnelling in our STM configuration differs from the case of planar junctions in that:

1. the capacitive energy E_C is much bigger than the Josephson energy, E_J, turning the environmental impedance into a relevant quantity;

2. the thermal energy is relatively high.

Figure 3.1d shows the equivalent circuit for a generic junction in an STM environment.
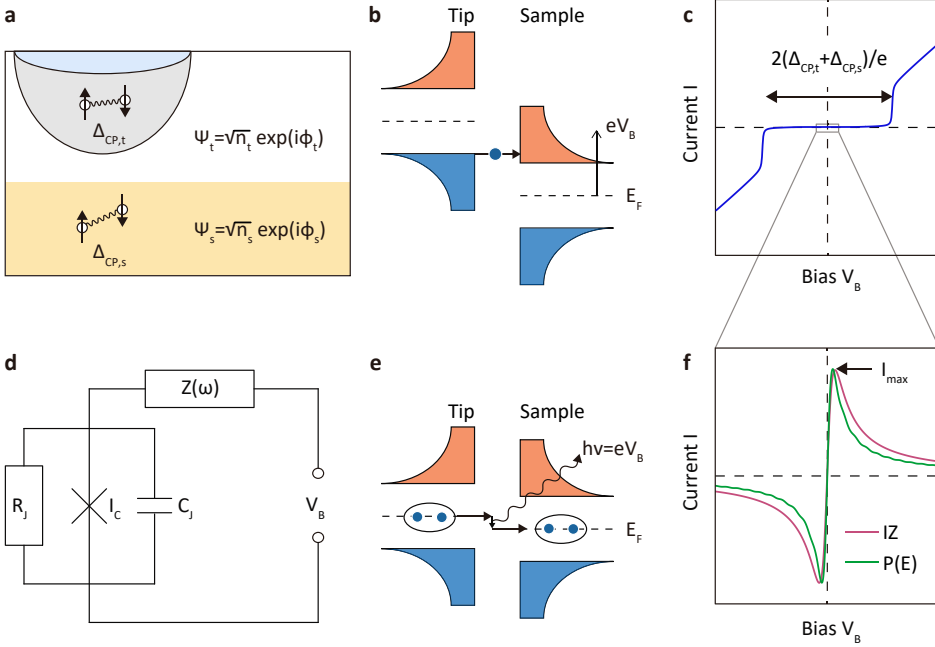
3

Figure 3.1: **Principes of Josephson Scanning Tunneling Microscopy. a** Schematic of a Josephson junction consisting of the tip and the sample. **b** Schematic energy diagram of quasiparticle tunnelling between the tip and the sample. Solid black lines indicate the density of states (horizontal axis) as a function of energy (vertical axis); filled (empty) states are denoted with blue (red); dashed lines indicate the Fermi level, E_F. When the voltage bias V_B is larger than $(\Delta_{CP,t} + \Delta_{CP,s})/e$, quasiparticles can tunnel (e is the electron charge). **c** Current–voltage characteristic curve (blue) for quasiparticle tunnelling. The dashed lines indicate zero values. The arrow indicates $2(\Delta_{CP,t} + \Delta_{CP,s})/e$. **d** Equivalent circuit diagram of the Josephson junction; the complex impedance $Z(\omega)$ represents the electromagnetic environment. **e** Schematic of inelastic Cooper pair tunnelling in a Josephson junction. A Cooper pair interacts with the environment by emitting energy of $h\nu = 2eV_B$ (wavy arrow; h, Planck constant; $\nu = \omega/2\pi$, frequency) and subsequently tunnels across the junction. **f** Simulated current–voltage curves for Cooper pair tunnelling, obtained using the IZ and $P(E)$ models. Both curves exhibit a maximum current I_{max} at a finite bias proportional to I_C^2 (I_C, critical supercurrent).

We calculate the current–voltage characteristics of Josephson tunnelling using two different theoretical frameworks: IZ and $P(E)$. The former (named after its developers, Ivanchenko and Zil'berman) models the environment as Ohmic and assumes that the thermal energy exceeds the Josephson energy [10]. The latter (named after the probability function, which is central to this theory) is a quantum mechanical treatment of Cooper pair tunnelling in ultrasmall junctions [11]. For our

3

configuration, the qualitative predictions obtained from both theoretical descriptions are similar: a Josephson current flows at small bias and exhibits a maximum within a few microvolts of the Fermi energy (Fig. 3.1e), which is reflected in a conductance spectrum that shows a peak at zero applied bias. The maximum Josephson current (arrow in Fig. 3.1f) is proportional to the square of the critical current I_C of the junction. In single-band, s-wave superconductors, the superfluid density is then proportional to $(I_C R_N)^2$, where R_N is the normal-state resistance, and is interpreted as the density of condensed Cooper pairs [12]. In multi-band or unconventional superconductors, the superfluid density defined this way represents the superposition of different contributions from different bands, with weights depending on the relative phase,

$$I_C R_N \propto \sum_i \sqrt{n_i} \cos(\chi_i), \tag{3.1}$$

where n_i are individual superfluid densities of the different bands and χ_i their relative phases (see also Appendix A). When tunnelling locally, one has to convert from a band basis to an orbital basis and consider the overlap of each kind of orbital with the different bands, as well as the individual tunnelling matrix elements for the different orbitals. One can still extract spatial variations in the superfluid using the definition above, if the ratios between the tunnelling matrix elements are spatially constant or when the superconducting phase is not strongly related to the orbitals. Importantly, the superfluid density thus defined cannot be simply interpreted as the total density of Cooper pairs for unconventional or multi-band superconductors, including the one investigated here. Notably, the multiplication with R_N in $(I_C R_N)^2$ further allows us to disentangle the measured superfluid density from variations in the coupling between the tip and the superfluid, which might vary spatially [13, 14]. Spatially imaging a superfluid using Josephson STM techniques [15] has thus far been achieved in two instances. First, a pair density wave was discovered in a copper oxide sample [13], by exfoliating pieces of the sample onto the STM tip and imaging it with a resolution of about 1 nm. Second, the superfluid of a Pb(111) surface was resolved with atomic resolution, by using the sample material to coat the STM tip [14].

3.3. Josephson tunneling on Fe(Te,Se)

In this study, we investigate the unconventional iron-based superconductor $FeTe_{0.55}Se_{0.45}$. Iron-based superconductors are moderately to strongly correlated, with Hund's rule and orbital selectivity playing important roles [16]. We chose $FeTe_{0.55}Se_{0.45}$ because it encompasses the key properties of unconventional superconductivity. Furthermore, its nodeless gap structure [17, 18] and the possibility to scan at low junction resistances facilitate Josephson experiments. $FeTe_{0.55}Se_{0.45}$ is considered not to be in the 'dirty' Bardeen–Cooper–Schrieffer (BCS) limit and has a low average superfluid density similar to that of copper oxide high-temperature superconductors [19, 20]. We cleave the single crystals at 30 K and insert the samples into our cryogenic STM system with rigorous electronic filtering (see Fig. 2.7). All measurements are performed at an effective electron temperature of 2.2 K. The topograph (Fig.

3.2a) shows atomic resolution and contrast differences that stem from the tellurium or selenium inhomogeneities; we further verify that the interstitial iron concentration is negligible. We use a mechanically sharpened platinum–iridium wire with its apex coated with lead, which is an s-wave superconductor with a relatively large gap [14] of about 1.3 meV. We characterize its properties on an atomically flat Pb(111) surface (see Appendix A and Fig. 2.7).
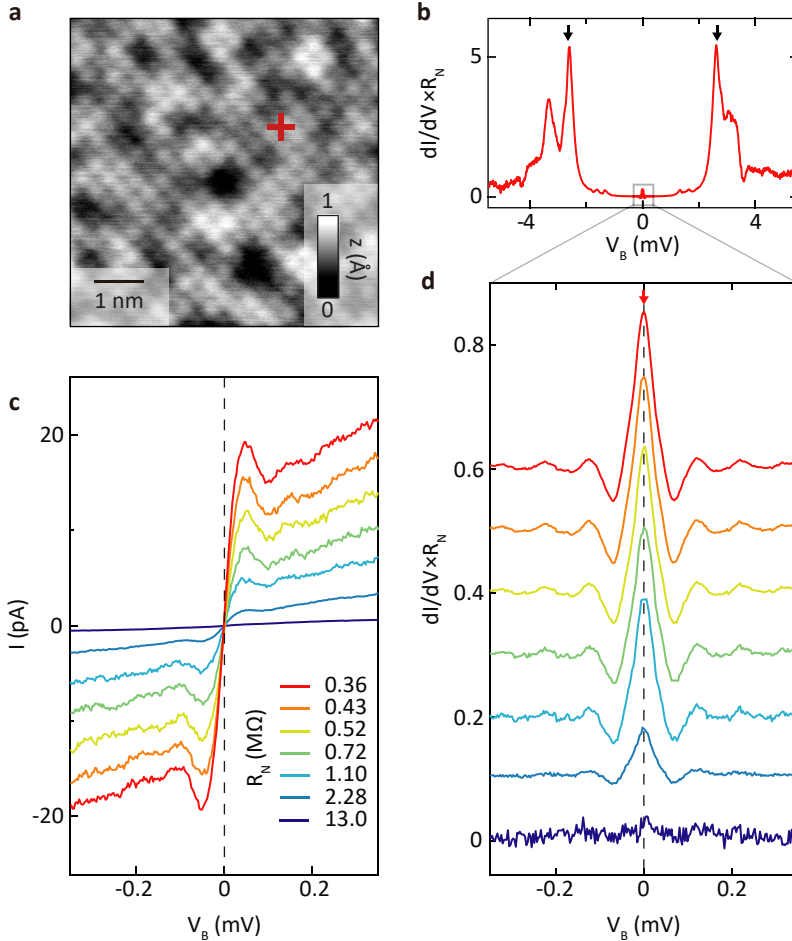

Figure 3.2: Josephson tunneling spectra on $FeTe_{0.55}Se_{0.45}$. **a** Atomically resolved topographic image (setup voltage, $V_{set} = -10$ mV; setup current, $I_{set} = 5$ nA). Brighter (darker) atoms correspond to Te (Se). **b** Differential conductance spectrum acquired at the location of the red cross in **a**, multiplied by the normal-state resistance. Black arrows indicate the coherence peaks. The Josephson current can be observed at small bias. Setup conditions: $V_{set} = -10$ mV; $I_{set} = 30$ nA; lock-in modulation, $V_{mod} = 20$ μV peak to peak. **c** Current–voltage characteristic curves for different normal-state resistances. All spectra are acquired with $V_{set} = -10$ mV. **d** Differential conductance spectra (acquired with the same setup conditions as in **c** and a lock-in modulation of $V_{mod} = 20$ μV peak to peak) multiplied by the respective normal-state resistance, yielding a dimensionless quantity.

These preparations enable us to acquire Josephson tunnelling spectra and maps on $FeTe_{0.55}Se_{0.45}$. Figure 3.2 shows current and differential conductance spectra acquired at the location marked by a cross in Fig. 3.2a. The data agree well with expectations from the IZ and $P(E)$ models, and reproduce small oscillation features seen previously in elemental superconductors and explained by a tip-induced antenna mode [14, 21]. Decreasing the junction resistance shows an increase in the critical current expected for a Josephson tunnelling junction (Fig. A.1). The rate of the increase is lower than that expected for simple s-wave junctions but more consistent with theoretical predictions for an $s_{\pm}$ pairing symmetry in the sample, where states with both positive and negative gaps tunnel [22]. We further note a small kink in the Josephson current at 25 μeV of yet unknown origin.

3.4. Mapping the superfluid in Fe(Te,Se)

In Fig. 3.3a, b we show an atomic-resolution map of the superfluid density as defined above, extracted from about 16000 individual spectra, as well as the topographic image, with the two images aligned to each other on the atomic scale at each point. The most striking finding of our experiment is the strong inhomogeneity of the superfluid over length scales of the order of the coherence length, that is, a few nanometres. To illustrate this, we show in Fig. 3.3c a series of individual raw spectra normalized by the normal-state resistance. The inhomogeneities are not periodic; a possible pair density wave with a small amplitude compared to the inhomogeneities would be below the sensitivity of our measurement. Our setup allows us to measure topographic and electronic properties in the same field of view and thus investigate possible causes for the inhomogeneity of the superfluid. The most obvious possible causes are structural disorder and strong quasiparticle scattering. The structural disorder stems from the effective FeSe and FeTe alloying, which is clearly visible in the topographic images (Figs. 3.2a, 3.3a). Surprisingly, the variations in the superfluid are not correlated to these structural features. The strength of the quasiparticle scattering is visible in the quasiparticle interference (QPI) pattern and is dominated by inter-pocket scattering in $FeTe_{0.55}Se_{0.45}$ (ref. [17]). In Fig. 3.3d we identify areas of strong scattering with red contours, which are obtained by Fourier-filtering the QPI data, to distinguish between strong- and weak-scattering regions. Again, there is no correlation between these regions and the superfluid density. We cannot exclude that the superfluid density is influenced by potential scatterers that are not visible in our measurement, remnant short-range magnetic order, or possible phase separations at higher energies. Given the putative $s_{\pm}$ pairing symmetry of the sample, as mentioned above, one could also consider a scenario involving spatially varying tunnelling matrix elements between the tip and orbitals that are coupled to gaps with opposite signs, leading to a spatially varying suppression of the Josephson current [22]. However, in $FeTe_{0.55}Se_{0.45}$ the gap sign is not strongly related to the orbital character [18, 23], and we do not observe the imprint that a relative change in the tunnelling matrix elements of the different orbitals would leave on the local density of states and the topography. More generally, the fact that prominent effects such as the chemical disorder and the inter-pocket QPI do not influence the superfluid indicates that the inhomogeneity
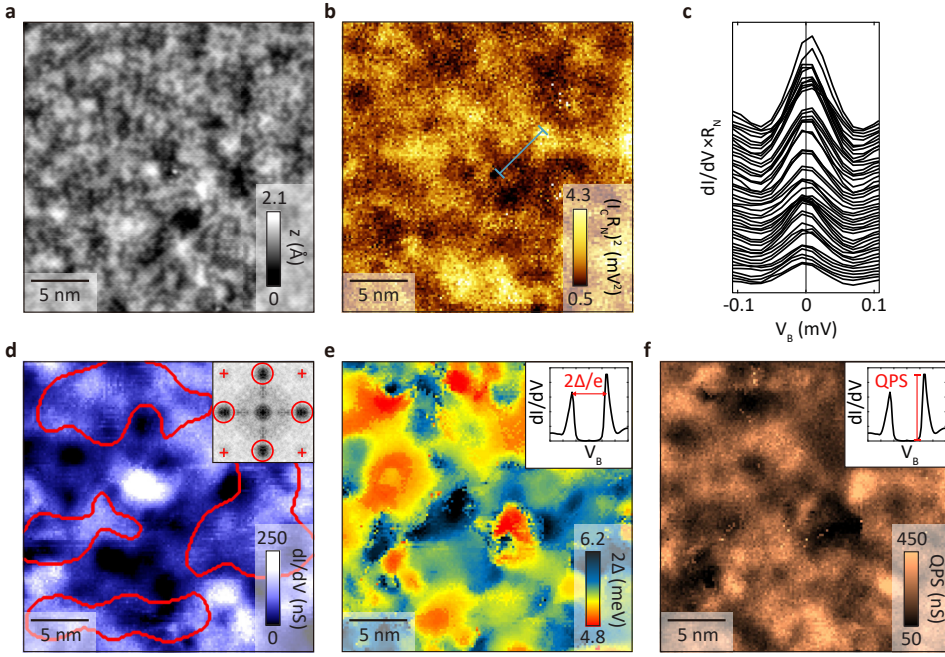
in the superfluid density is intrinsic.

Figure 3.3: **Visualizing the superfluid in** $FeTe_{0.55}Se_{0.45}$. **a** 25×25 nm^2 topographic image of $FeTe_{0.55}Se_{0.45}$ ($V_{set} = -6$ mV, $I_{set} = 0.12$ nA). **b** Spatially resolved map of $(I_C R_N)^2$, representing the superfluid density as discussed in the text ($V_{set} = -6$ mV, $I_{set} = 5$ nA, $V_{mod} = 30$ μV peak to peak). **c** Series of differential conductance spectra obtained along the blue line in **b**, multiplied by the normal-state resistance around E_F. **d** Conductance map at $V_B = +3.6$ mV. Areas with strong quasiparticle interference patterns are marked by red contours, which are obtained by Fourier filtering of the QPI data using the filter shown in the inset (red circles). Inset: Fourier transform; crosses indicate Bragg peak locations. **e** Pair-breaking gap map, with $\Delta = \Delta_{CP,t} + \Delta_{CP,s}$; the inset shows a typical spectrum. **f** Coherence peak-height map (QPS), extracted simultaneously with the pair-breaking gap, as indicated in the inset. All maps in **b–f** were obtained in the same field of view as that used for the topograph in **a**, and the images are aligned to each other at each point using the simultaneously acquired topographs. The setup conditions for **d–f** are $V_{set} = -6$ mV, $I_{set} = 0.3$ nA and $V_{mod} = 400$ μV peak to peak.

We now return to the relation between the pair-breaking gap and the superfluid density. We extract the pair-breaking gap energy, as well as the height of the coherence peaks (which will prove to be important later) by fitting the coherence peaks of each spectrum to find the energy of the maxima. Figure 3.3e shows the gap map for the same field of view as that used for the Josephson map. The gap variations agree with previous reports [24]. It is clear that the pair-breaking gap is independent of the superfluid density; instead, we find a correlation to the quasiparticle character, as described below.

3.5. Superfluid density-quasiparticle strength correlation

In unconventional superconductors, there is a recurring theme that connects quasiparticle excitation line shapes with the presence of superconductivity: photoemission demonstrates that incoherent quasiparticles in the normal state become coherent below the critical temperature [18, 25], T_C. Previous STM measurements showed Bogoliubov QPI patterns at low energies that were even sharper than theory would predict but vanished well below the gap energy [26]. Those measurements suggested a remarkable relation between the average quasiparticle excitation spectrum and superconductivity, but did not address the inhomogeneous character of unconventional superconductors. Although recently a relation between superfluid density and quasiparticle character has been conjectured to hold also locally for single-layer copper oxides [27], direct experimental evidence is so far missing. Our measurement allows us to extract the quasiparticle strength (QPS), which we define phenomenologically as the height of the coherence peak (Fig. 3.3f), and relate it directly to the superfluid density at the same location. Indeed, we find a striking correlation between the superfluid density and the QPS over the whole field of view, with a linear correlation coefficient of 0.58 (Fig. 3.4). Although this phenomenology cannot be explained by an existing theory, it points towards a local mechanism behind the relation found from photoemission measurements—a condition fulfilled by pinned thermal phase fluctuations and glassy superconductivity [1, 28].
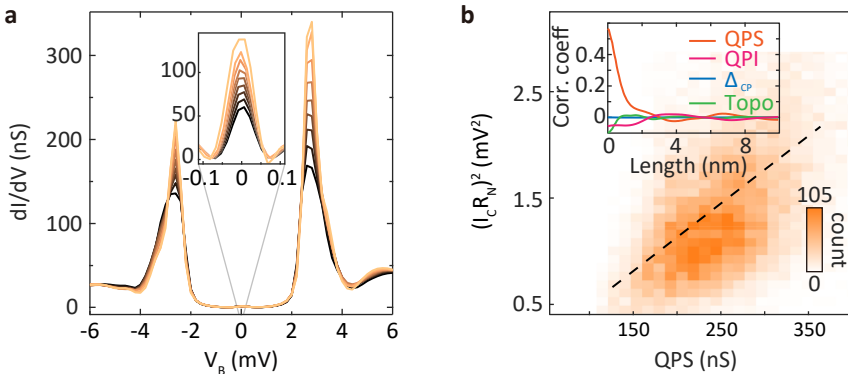

Figure 3.4: **Correlation between** $(I_C R_N)^2$ **and coherence peak height. a** Sorted spectra of the coherence peak height ($V_{set} = -6$ mV, $I_{set} = 0.3$ nA) and the zero-bias Josephson peak (inset: $V_{set} = -6$ mV, $I_{set} = 5$ nA). The spectra were sorted by binning of the superfluid density map shown in Fig. 3.3b. The colours correspond to the quasiparticle strength indicated by the colour bar in Fig. 3.3f. **b** Correlation between the coherence peak height and the superfluid density extracted from $(I_C R_N)2$ as discussed in the text, yielding a correlation factor of 0.58 (dashed line). The inset shows the distance dependence of the correlation factors between the superfluid density and QPS, QPI, Δ_{CP} and the topographic height (see Fig. A.4).

The length scales of the superfluid inhomogeneity and of its correlation to the QPS (Fig. 3.4b, inset) are of the same order as the average electron–electron dis-

tance. Therefore, our measurement indicates that the Cooper pairs in $FeTe_{0.55}Se_{0.45}$ are very local: they are small in size and have little overlap compared with those in conventional superconductors. We can further compare this situation to the crossover from momentum-condensed pairs described by BCS theory to completely local pairs described by Bose–Einstein condensation (BEC), which has been demonstrated with ultracold atomic gases for s-wave superfluids [29, 30]. There also exist indications for pairing in the BEC or crossover regime close to superconductor–insulator transitions and in copper oxides; in $FeTe_{0.55}Se_{0.45}$ the phenomenology is not conclusive [18, 31]. Although our data point towards the formation of local pairs in $FeTe_{0.55}Se_{0.45}$, we note that in a multi-band, putative sign-changing superconductor, we expect the situation to be more complicated than the realization seen in ultracold atomic gases, and both better theory and more experiments are needed.

3.6. Conclusions and outlook

In summary, we detected and directly imaged a strongly inhomogeneous superfluid and simultaneously measured the electronic and topographic properties in the same field of view, with atomic resolution. We found that the inhomogeneity of the superfluid is not caused by structural disorder resulting from the Se/Te alloying, by inter-pocket scattering or by variations of the pair-breaking gap energy (Fig. 3.4b, inset). Instead, the superfluid density shows strong positive correlation with the sharpness of the quasiparticle peak: superconductivity appears to be needed for coherent quasiparticles locally, on the length scale of Cooper pairing. It will be instructive to use the techniques described here to investigate the superfluid density in other materials, including superconductor–insulator transitions, disordered conventional superconductors or twisted bilayer graphene [32, 33]. Lastly, we anticipate that future temperature-dependent superfluid density and gap measurements will elucidate what local and global mechanisms limit T_C in unconventional superconductors.

References

[1] V. Emery and S. Kivelson, *Importance of phase fluctuations in superconductors with small superfluid density,* Nature **374**, 434 (1995).

[2] B. Keimer, S. A. Kivelson, M. R. Norman, S. Uchida, and J. Zaanen, *From quantum matter to high-temperature superconductivity in copper oxides,* Nature **518**, 179 (2015).

[3] P. Fulde and R. A. Ferrell, *Superconductivity in a strong spin-exchange field,* Phys. Rev. **135**, A550 (1964).

[4] A. Larkin and Y. N. Ovchinnikov, *Nonuniform state of superconductors,* Sov. Phys.-JETP **20**, 762 (1965).

[5] A. Ghosal, M. Randeria, and N. Trivedi, *Spatial inhomogeneities in disordered d-wave superconductors,* Phys. Rev. B **63**, 020505 (2000).

[6] M. Feigel'Man and L. Ioffe, *Superfluid density of a pseudogapped superconductor near the superconductor-insulator transition,* Phys. Rev. B **92**, 100509 (2015).

[7] K. Bouadim, Y. L. Loh, M. Randeria, and N. Trivedi, *Single-and two-particle energy gaps across the disorder-driven superconductor–insulator transition,* Nat. Phys. **7**, 884 (2011).

[8] F. Wang and D.-H. Lee, *The electron-pairing mechanism of iron-based superconductors,* Science **332**, 200 (2011).

[9] I. Božović, J. Wu, X. He, and A. Bollinger, *What is really extraordinary in cuprate superconductors?* Physica C **558**, 30 (2019).

[10] Y. Ivanchenko and L. Zil'Berman, *The Josephson effect in small tunnel contacts,* Sov. Phys. JETP **28** (1969).

[11] G.-L. Ingold, H. Grabert, and U. Eberhardt, *Cooper-pair current through ultrasmall Josephson junctions,* Phys. Rev. B **50**, 395 (1994).

[12] O. Naaman, W. Teizer, and R. Dynes, *Fluctuation dominated Josephson tunneling with a scanning tunneling microscope,* Phys. Rev. Lett. **87**, 097004 (2001).

[13] M. Hamidian, S. Edkins, S. H. Joo, A. Kostin, H. Eisaki, S. Uchida, M. Lawler, E.-A. Kim, A. Mackenzie, K. Fujita, *et al.*, *Detection of a Cooper-pair density wave in $Bi_2Sr_2CaCu_2O_{8+x}$,* Nature **532**, 343 (2016).

[14] M. T. Randeria, B. E. Feldman, I. K. Drozdov, and A. Yazdani, *Scanning Josephson spectroscopy on the atomic scale,* Phys. Rev. B **93**, 161115 (2016).

[15] M. Graham and D. K. Morr, *Imaging the spatial form of a superconducting order parameter via Josephson scanning tunneling spectroscopy,* Phys. Rev. B **96**, 184501 (2017).

[16] Z. Yin, K. Haule, and G. Kotliar, *Kinetic frustration and the nature of the magnetic and paramagnetic states in iron pnictides and iron chalcogenides,* Nat. Mater. **10**, 932 (2011).

[17] T. Hanaguri, S. Niitaka, K. Kuroki, and H. Takagi, *Unconventional s-wave superconductivity in Fe (Se, Te),* Science **328**, 474 (2010).

[18] H. Miao, W. Brito, Z. Yin, R. Zhong, G. Gu, P. Johnson, M. Dean, S. Choi, G. Kotliar, W. Ku, *et al.*, *Universal 2 $\Delta_{\max}/k_B T_c$ scaling decoupled from the electronic coherence in iron-based superconductors,* Phys. Rev. B **98**, 020502 (2018).

[19] C. Homes, Y. Dai, J. Wen, Z. Xu, and G. Gu, *FeTe$_{0.55}$Se$_{0.45}$: A multiband superconductor in the clean and dirty limit,* Phys. Rev. B **91**, 144503 (2015).

[20] M. Bendele, S. Weyeneth, R. Puzniak, A. Maisuradze, E. Pomjakushina, K. Conder, V. Pomjakushin, H. Luetkens, S. Katrych, A. Wisniewski, *et al.*, *Anisotropic superconducting properties of single-crystalline FeSe$_{0.5}$Te$_{0.5}$,* Phys. Rev. B **81**, 224520 (2010).

[21] B. Jäck, M. Eltschka, M. Assig, A. Hardock, M. Etzkorn, C. R. Ast, and K. Kern, *A nanoscale gigahertz source realized with Josephson scanning tunneling microscopy,* Appl. Phys. Lett. **106**, 013109 (2015).

[22] Y. Ota, N. Nakai, H. Nakamura, M. Machida, D. Inotani, Y. Ohashi, T. Koyama, and H. Matsumoto, *Ambegaokar-Baratoff relations for Josephson critical current in heterojunctions with multigap superconductors,* Phys. Rev. B **81**, 214511 (2010).

[23] Z. Liu, M. Yi, Y. Zhang, J. Hu, R. Yu, J.-X. Zhu, R.-H. He, Y. Chen, M. Hashimoto, R. Moore, *et al.*, *Experimental observation of incoherent-coherent crossover and orbital-dependent band renormalization in iron chalcogenide superconductors,* Phys. Rev. B **92**, 235138 (2015).

[24] U. R. Singh, S. C. White, S. Schmaus, V. Tsurkan, A. Loidl, J. Deisenhofer, and P. Wahl, *Spatial inhomogeneity of the superconducting gap and order parameter in FeSe$_{0.4}$Te$_{0.6}$,* Phys. Rev. B **88**, 155124 (2013).

[25] D. Feng, D. Lu, K. Shen, C. Kim, H. Eisaki, A. Damascelli, R. Yoshizaki, J.-i. Shimoyama, K. Kishio, G. Gu, *et al.*, *Signature of superfluid density in the single-particle excitation spectrum of Bi$_2$Sr$_2$CaCu$_2$O$_{8+\delta}$,* Science **289**, 277 (2000).

[26] Y. Kohsaka, C. Taylor, P. Wahl, A. Schmidt, J. Lee, K. Fujita, J. Alldredge, K. McElroy, J. Lee, H. Eisaki, *et al.*, *How Cooper pairs vanish approaching the Mott insulator in Bi$_2$Sr$_2$CaCu$_2$O$_{8+\delta}$,* Nature **454**, 1072 (2008).

[27] W. Ruan, X. Li, C. Hu, Z. Hao, H. Li, P. Cai, X. Zhou, D.-H. Lee, and Y. Wang, *Visualization of the periodic modulation of Cooper pairing in a cuprate superconductor,* Nat. Phys. **14**, 1178 (2018).

3

[28] Y. Dubi, Y. Meir, and Y. Avishai, *Nature of the superconductor–insulator tran-sition in disordered superconductors,* Nature **449**, 876 (2007).

[29] I. Bloch, J. Dalibard, and W. Zwerger, *Many-body physics with ultracold gases,* Rev. Mod. Phys. **80**, 885 (2008).

[30] M. Randeria and E. Taylor, *Crossover from Bardeen-Cooper-Schrieffer to Bose-Einstein condensation and the unitary Fermi gas,* Annu. Rev. Condens. Matter Phys. **5**, 209 (2014).

[31] B. Sacépé, T. Dubouchet, C. Chapelier, M. Sanquer, M. Ovadia, D. Shahar, M. Feigel'Man, and L. Ioffe, *Localization of preformed Cooper pairs in disor-dered superconductors,* Nat. Phys. **7**, 239 (2011).

[32] Y. Cao, V. Fatemi, S. Fang, K. Watanabe, T. Taniguchi, E. Kaxiras, and P. Jarillo-Herrero, *Unconventional superconductivity in magic-angle graphene superlattices,* Nature **556**, 43 (2018).

[33] N. Reyren, S. Thiel, A. Caviglia, L. F. Kourkoutis, G. Hammerl, C. Richter, C. W. Schneider, T. Kopp, A.-S. Rüetschi, D. Jaccard, *et al.*, *Superconducting interfaces between insulating oxides,* Science **317**, 1196 (2007).

3